Signals of quark combination at hadronization in pp collisions at $\sqrt{s} = 200$ GeV

Jun Song,[1] Hai-hong Li,[1] and Feng-lan Shao[2,*]

[1]*School of Physical Science and Intelligent Engineering, Jining University, Shandong 273155, China*
[2]*School of Physics and Physical Engineering, Qufu Normal University, Shandong 273165, China*

(Received 6 October 2021; accepted 8 April 2022; published 25 April 2022)

We find signals of quark combination at hadronization from the experimental data of p_T spectra of hadrons at midrapidity in pp collisions at $\sqrt{s} = 200$ GeV. The first is the constituent quark number scaling property for p_T spectra of Ω^- and ϕ and that for p_T spectra of p and ρ^0. The second is that p_T spectra of Λ, Ξ^-, and K^{*0} can be self-consistently described using the spectrum of strange quarks from ϕ data and that of up/down quarks from p data in the equal-velocity combination mechanism. The third is that experimental data for p_T spectrum of D^{*+} are also well described by the spectrum of up/down quarks from p data and a spectrum of charm quarks which is consistent with theoretical calculations of the fixed-order next-to-leading-logarithmic approach. These results indicate a similarity between hadron production in pp collisions at $\sqrt{s} = 200$ GeV and that at LHC energies. We predict p_T spectra of single-charm hadrons and their spectrum ratios. We suggest systematic measurements in pp collisions at $\sqrt{s} = 200$ GeV in the future so as to better understand the property of the small parton system created in pp collisions at different collision energies.

DOI: 10.1103/PhysRevD.105.074027

I. INTRODUCTION

Hadronization refers to the process of the formation of hadrons from final-state quarks and gluons created in high energy reactions. Hadronization is a nonperturbative quantum chromodynamics (QCD) process and is described by phenomenological models at present. String fragmentation [1], cluster fragmentation [2], and quark recombination [3,4] are three kinds of popular models which are often used to describe the hadron production in high energy reactions.

Experimental data of hadron production in high energy reactions often provide new inspiration for the understanding of hadronization. We recall that heavy-ion collision experiments at the Relativistic Heavy Ion Collider (RHIC) in the 2000s found several surprising phenomena such as the enhanced baryon-to-meson ratio [5–7] and the number of constituent quark scaling properties for hadronic elliptic flow [8–10] in the intermediate p_T range. These observations prompt the study of quark (re)combination or the parton coalescence mechanism [11–16] for the hadronization of bulk quark matter created in relativistic heavy-ion collisions. On the other hand, the hadronization of a parton jet with high p_T and a small parton system is still usually described by the fragmentation mechanism.

In the last decade, experiments of pp and pA collisions at energies available at the Large Hadron Collider (LHC) found a series of new phenomena in hadron production in high multiplicity events such as ridge or long-range correlation [17,18], collectivity [19,20], and enhanced baryon-to-meson ratio [21–24]. These phenomena have been observed in relativistic heavy-ion collisions and are usually regarded to be closely related to the formation of quark-gluon plasma (QGP). Observation of these phenomena in pp and pA collisions at the LHC therefore invoke an interesting question, i.e., the possible creation of mini-QGP. Theoretical studies of the underlying dynamics in small collision systems at LHC energies are intensively carried out, which usually focus on the hydrodynamic evolution of the created soft parton system [25–30], multiple parton interactions [31], color reconnection and related phenomenological mechanisms [32–36], string and cluster fragmentation [37,38], statistical hadronization model for hadron production [39], etc. Our recent studies [40–46] found that an equal-velocity combination (EVC) mechanism of constituent quarks and antiquarks at hadronization can systematically describe p_T spectra of light-flavor and single-charm hadrons. Compared with the traditional viewpoint that the fragmentation mechanism is often applied to a small parton system and usually successful, our studies

*shaofl@mail.sdu.edu.cn

indicate the new feature of hadron production at hadronization in pp and pA collisions at LHC energies.

The production of identified hadrons in pp collisions at $\sqrt{s} = 200$ GeV was systematically measured by the STAR Collaboration in the early years of RHIC experiments [47–53]. Experimental data were usually compared with calculations of event generators such as PYTHIA with tuned parameters. In view of our findings in pp collisions at LHC energies [40–46], it is interesting to study the performance of the quark combination in pp collisions at $\sqrt{s} = 200$ GeV so as to find the similarity or difference in hadron production in pp collisions at two collision energy scales. The study of p_T spectra of identified hadrons in this paper gives a surprising indication.

II. QUARK NUMBER SCALING OF HADRONIC p_T SPECTRA

In this paper, we apply a particular quark combination model [41,42] to study p_T spectra of hadrons in pp collisions. In this model, we assume the constituent quarks and antiquarks as the effective degrees of freedom for the final-state parton systems created in pp collisions. We apply the constituent quark model to describe the internal structure of hadrons at the low energy scale. Then, at hadronization the combination of these constituent quarks and antiquarks created in collisions can directly form the hadron. We take the EVC approximation; i.e., the hadron is formed by constituent quarks and antiquarks with equal velocity. To qualify this approximation, we take the constituent quark masses so that the summation of constituent masses of (anti)quarks approximately equals the rest mass of the hadrons; i.e., the EVC of the constituent (anti)quarks can correctly construct on-shell hadrons. Under EVC approximation, the momentum spectra of hadrons have analytical and simple formulas, from which we can build some scaling properties that can be conveniently tested by experimental data.

In our EVC model, p_T distribution of a hadron ($dN/dp_T dy$) at midrapidity is the product of those of (anti)quarks

$$f_{B_i}(p_T) = \kappa_{B_i} f_{q_1}(x_1 p_T) f_{q_2}(x_2 p_T) f_{q_3}(x_3 p_T), \quad (1)$$

$$f_{M_i}(p_T) = \kappa_{M_i} f_{q_1}(x_1 p_T) f_{\bar{q}_2}(x_2 p_T). \quad (2)$$

The moment fractions satisfy $x_1 + x_2 + x_3 = 1$ with $x_i = m_i/(m_1 + m_2 + m_3)$ $(i = 1, 2, 3)$ in baryon formation and $x_1 + x_2 = 1$ with $x_i = m_i/(m_1 + m_2)$ $(i = 1, 2)$ in meson formation. m_i is the constituent mass of quark q_i. Coefficients κ_{B_i} and κ_{M_i} are independent of p_T but dependent on the numbers of quarks and antiquarks [42].

For hyperon $\Omega^-(sss)$, which only consists of strange quarks, its p_T distribution has a simple expression

$$f_\Omega(p_T) = \kappa_\Omega [f_s(p_T/3)]^3. \quad (3)$$

The p_T distribution of the meson $\phi(s\bar{s})$ also has a simple expression

$$f_\phi(p_T) = \kappa_\phi f_s(p_T/2) f_{\bar{s}}(p_T/2) = \kappa_\phi [f_s(p_T/2)]^2, \quad (4)$$

where the approximation $f_s(p_T) = f_{\bar{s}}(p_T)$ at midrapidity is taken. From Eqs. (3) and (4), we obtain a relationship

$$f_\phi^{1/2}(2p_T) = \kappa_{\phi,\Omega} f_\Omega^{1/3}(3p_T), \quad (5)$$

which is called the constituent quark number scaling of hadronic p_T spectra. The coefficient $\kappa_{\phi,\Omega} = \kappa_\phi^{1/2}/\kappa_\Omega^{1/3}$ is independent of p_T. For p_T spectra of the proton and ρ, we obtain a similar relationship

$$f_\rho^{1/2}(2p_T) = \kappa_{\rho,p} f_p^{1/3}(3p_T), \quad (6)$$

where approximations $f_u(p_T) = f_d(p_T)$ and $f_u(p_T) = f_{\bar{u}}(p_T)$ at midrapidity are taken. We run PYTHIA8 with default parameter values and find that the calculation results do not exhibit properties in Eqs. (5) and (6).

In Fig. 1(a), we test the scaling property Eq. (5) using the experimental data of $\Omega^- + \bar{\Omega}^+$ and ϕ at midrapidity in inelastic pp collisions at $\sqrt{s} = 200$ GeV [47,50]. $\kappa_{\phi,\Omega}$ is taken as 1.88. $\Omega^- + \bar{\Omega}^+$ has only three datum points, and we see that they are almost coincident with the scaled data of ϕ. In Fig. 1(b), we test Eq. (6) using the experimental data of the proton and ρ^0 [48,51]. $\kappa_{\rho,p}$ is taken as 1.10. Except for the first datum point at $p_{T,u} \approx 0.15$ GeV/c, we see that other datum points of ρ^0 are very close to the scaled data of the proton. We emphasize that the values of the two coefficients $\kappa_{\phi,\Omega}$ and $\kappa_{\rho,p}$ can be reproduced in our model by considering quark number distributions at hadronization. Therefore, these two scaling tests positively indicate a quark combination mechanism at hadronization in pp collisions even at $\sqrt{s} = 200$ GeV.

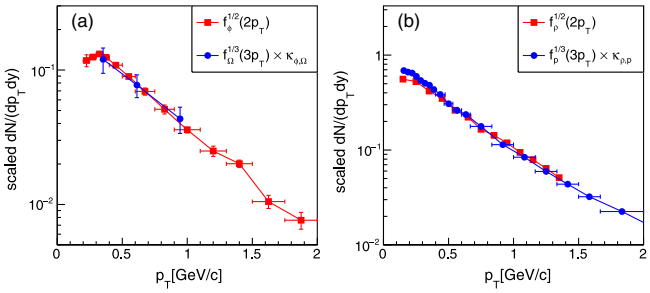

FIG. 1. Test of the quark number scaling property for p_T spectra of Ω and ϕ (a) and those of ρ^0 and proton (b) at midrapidity in pp collisions at $\sqrt{s} = 200$ GeV by using experimental data of the STAR Collaboration [47,48,50,51]. $\kappa_{\phi,\Omega}$ is 1.88 and $\kappa_{\rho,p}$ is 1.10.The line between the datum points is to guide the eye along the shape of the scaled data.

III. p_T SPECTRA OF MIXING-FLAVOR HADRONS

We understand the experimental data for p_T spectra of Λ, Ξ^-, and K^{*0} [49,50] at midrapidity in pp collisions at $\sqrt{s} = 200$ GeV. These hadrons consist of strange quarks and up/down quarks. By Eqs. (1) and (2), their p_T spectra at hadronization are given as

$$f_\Lambda(p_T) = \kappa_\Lambda \left[f_u\left(\frac{1}{2+r_{su}} p_T\right)\right]^2 f_s\left(\frac{r_{su}}{2+r_{su}} p_T\right), \quad (7)$$

$$f_\Xi(p_T) = \kappa_\Xi \left[f_s\left(\frac{r_{su}}{1+2r_{su}} p_T\right)\right]^2 f_u\left(\frac{1}{1+2r_{su}} p_T\right), \quad (8)$$

$$f_{K^*}(p_T) = \kappa_{K^*} f_u\left(\frac{1}{1+r_{su}} p_T\right) f_s\left(\frac{r_{su}}{1+r_{su}} p_T\right), \quad (9)$$

where $r_{su} = m_s/m_u$ is the relative momentum ratio of the strange quark to up quark. Because the constituent masses of quarks $m_s = 0.5$–0.55 GeV and $m_u = 0.3$–0.33 GeV have some uncertainties, the ratio r_{su} is about $5/3$ with approximately $\pm 10\%$ degrees of freedom. Our numerical results show that the p_T spectra that are above the hadrons are not sensitive to this magnitude change of r_{su}. Therefore, in this paper, we only present the calculation results for the p_T spectra that are above the hadrons at $r_{su} = 1.67$ as typical predictions of our model.

To calculate Eqs. (7)–(9), quark distributions $f_s(p_T)$ and $f_u(p_T)$ at hadronization are needed. We obtain them by using our EVC model to fit the experimental data of the ϕ and proton [47,50], and the results are shown in Fig. 2. Here, the decay contributions of the decuplet baryons in the ground state to octet baryons are included. The expression of the coefficient κ_h and its derivation in the EVC model can be found in Refs. [42,43,46].

In Fig. 3(a), we first show the p_T spectrum of ρ^0 at midrapidity based on $f_u(p_T)$ fitted from the proton data. We see that the ρ^0 result is in good agreement with the experimental data [48]. We note that the consistency between the ρ^0 and proton here is better than the scaling test in Fig. 1(b). This is because the final-state protons receive certain decay contamination of the decuplet baryons Δ, which will weakly influence the p_T spectrum of the proton. Ω and ϕ hardly contain decay contributions, and therefore, their p_T spectra do not have this contamination.

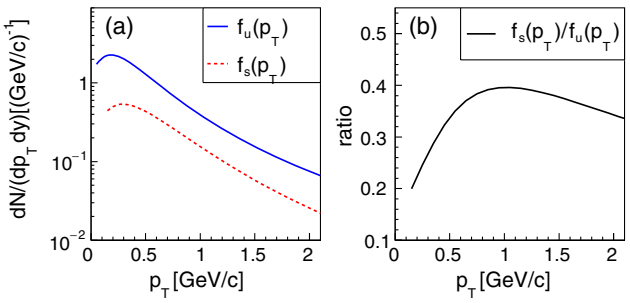

FIG. 2. p_T spectra of strange and up quarks at midrapidity (a) and their spectrum ratio (b) in pp collisions at $\sqrt{s} = 200$ GeV.

In Fig. 3(b), we show the results for the p_T spectra of Λ, Ξ^-, and K^{*0} at midrapidity. We see good agreement with the experimental data of the three hadrons [49,50]. Combining the results of Figs. 1 and 3, we see that the experimental data of ϕ, Ω^-, ρ^0, proton, Λ, Ξ^-, and K^{*0} can be self-consistently explained by a set of quark spectra at hadronization $f_u(p_T)$ and $f_s(p_T)$ under the equal-velocity combination mechanism. This is the explicit signal of a quark combination at hadronization in pp collisions at $\sqrt{s} = 200$ GeV.

IV. p_T SPECTRUM OF SINGLE-CHARM HADRON D^{*+}

We now extend the above study to the combination of a charm quark and light-flavor quarks. Because the constituent mass of a charm quark is larger than that of light-flavor quarks, a charm quark with momentum p_T will hadronize by combining a light-flavor antiquark or two light-flavor quarks with momentum p_T/r_{cl} where $r_{cl} = m_c/m_l$ $(l = u, s)$. In our EVC model, the p_T distribution of D^{*+} is

$$f_{D^*}(p_T) = \kappa_{D^*} f_c\left(\frac{r_{cu}}{1+r_{cu}} p_T\right) f_u\left(\frac{1}{1+r_{cu}} p_T\right), \quad (10)$$

where we assume $f_u(p_T) = f_{\bar{u}}(p_T)$ at midrapidity.

Momentum fractions r_{cu} and r_{cs} have about $\pm 10\%$ degrees of freedom because of the uncertainty of the constituent mass of charm quark $m_c = 1.5$–1.7 GeV and those of light-flavor quarks $m_s = 0.5$–0.55 GeV and $m_u = 0.3$–0.33 GeV. We have checked that the numerical results for p_T spectra of single-charm hadrons are not sensitive to this freedom. Therefore, in this paper, we only present the calculation results for p_T spectra of single-charm hadrons at $r_{cu} = 5$ and $r_{cs} = 3$ as typical predictions of our model.

Since $f_u(p_T)$ is already known by fitting the data of the proton, the p_T spectrum of D^{*+} can be calculated when $f_c(p_T)$ is also given. Here, we adopt a perturbative QCD calculation for a differential cross section of charm quarks from the fixed-order next-to-leading-logarithmic (FONLL) approach [54,55] and obtain the p_T spectrum of charm quarks at midrapidity by an online calculator[1] with the CTEQ6.6 parton distribution function. The result of $d\sigma_c/(dp_T dy)$ is shown as the dotted line in Fig. 4(a) where the shadow area denotes the theoretical uncertainties (quadratic combination of scale and mass uncertainties).

[1]FONLL online calculator at http://www.lpthe.jussieu.fr/~cacciari/fonll/fonllform.html.

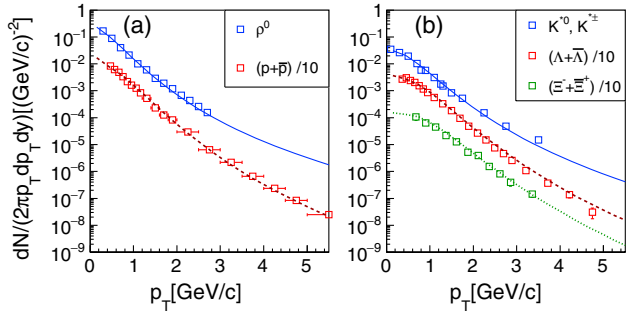

FIG. 3. p_T spectra of ρ^0 and proton (a) and those of strange hadrons (b) at midrapidity in pp collisions at $\sqrt{s} = 200$ GeV. Lines are model results and symbols are experimental data [49,50].

Applying this charm quark distribution, we calculate the p_T spectrum of D^{*+} by Eq. (10) and show the result as the dotted line in Fig. 4(b) where the shadow area denotes the uncertainties inherited from those of the charm quarks. We see that the experimental data of D^{*+} [52,53], open square and circle symbols, are higher than our dotted line, which is calculated from the central values of the charm quark distribution and are systematically close to the upper boundary of the uncertainty band. We note that this feature was also observed in pp collisions at LHC energies in our previous works with quark combination hadronization [45,46] and FONLL calculations with fragmentation functions at both RHIC and LHC energies [52,56–58].

In order to focus on the test of our model without interference from the relatively large uncertainties of charm quark distribution shown in Fig. 4(a), we choose a particular charm quark distribution in the following calculations of single-charm hadrons. The distribution is close to the upper boundary of the FONLL calculations so as to reproduce the data of D^{*+} and is still within the theoretical uncertainties. It is shown as the solid line in Fig. 4(a) and can be parametrized as $f_c(p_T) = \frac{d\sigma_c}{dy} f_c^{(n)}(p_T)$ with

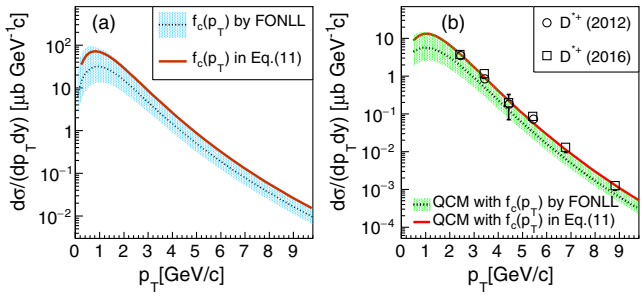

FIG. 4. (a) The charm quark distribution in pp collisions at $\sqrt{s} = 200$ GeV. The dotted line with the uncertainty band is calculated by FONLL. (b) Differential cross section of D^{*+} at midrapidity. Symbols are experimental data of D^{*+} [52,53]. The dotted line with the uncertainty band is the model result of D^{*+} when we directly apply the charm quark distribution given by FONLL calculations. The solid line in (b) is the model result of D^{*+} when we apply a particular charm quark distribution shown as the solid line in (a). See text for details.

$$f_c^{(n)}(p_T) = \mathcal{N} p_T \left(1 + \frac{\sqrt{p_T^2 + M^2} - M}{nC}\right)^{-n}, \quad (11)$$

where $\mathcal{N} = [(n-1)(n-2)]/[nC[nC + M(n-2)]]$ is a normalization coefficient, $n = 9.66$, $M = 1.5$ GeV, and $C = 0.38$ GeV. The p_T integrated cross section is taken to be $d\sigma_c/dy = 125$ μb which is close to the upper edge of the FONLL calculation $d\sigma_c/dy = 59^{+88}_{-31}$ μb. The p_T spectrum of D^{*+} calculated from this charm quark distribution is shown as the solid line in Fig. 4(b). In the following studies, we calculate the p_T spectra of other single-charm hadrons with this charm quark distribution and take them as typical predictions of our model.

V. PREDICTION OF SINGLE-CHARM HADRONS

We now study the combination of a charm quark with a strange antiquark to form a D_s^+. The calculation results for the differential cross section of D_s^+ and the spectrum ratio $D_s^+/(D^0 + D^+)$ as a function of p_T are shown in Fig. 5. Compared with $D^{0,+}$, the production of D_s^+ is suppressed. As we know, in the light-flavor background the number of strange (anti)quarks is smaller than that of up/down (anti) quarks. Therefore, a charm has a relatively small chance to capture a comoving $\bar{s}$ to form a D_s^+. We use a suppression factor $\lambda_s = N_s/N_{\bar{u}}$ to denote the relative abundance of strange quarks. In our model, the yield ratio of $D_s^+/(D^0 + D^+)$ at midrapidity has a simple expression

$$\frac{d\sigma_{D_s^+}/dy}{d\sigma_{D^0+D^+}/dy} = \frac{1}{2}\lambda_s. \quad (12)$$

With the obtained $f_s(p_T)$ and $f_u(p_T)$ in Fig. 2(a) in the study of light-flavor hadrons in Sec. III, we have $\lambda_s = 0.29$ in pp collisions at $\sqrt{s} = 200$ GeV. Therefore, we see in Fig. 5(b) that the spectrum ratio $D_s^+/(D^0 + D^+)$ is located in the range [0.1,0.2]. We further see that the spectrum ratio is dependent on p_T to a certain extent. This is because the relative abundance of strange quarks is p_T dependent [see the result of $f_s(p_T)/f_u(p_T)$ in Fig. 2(b)],

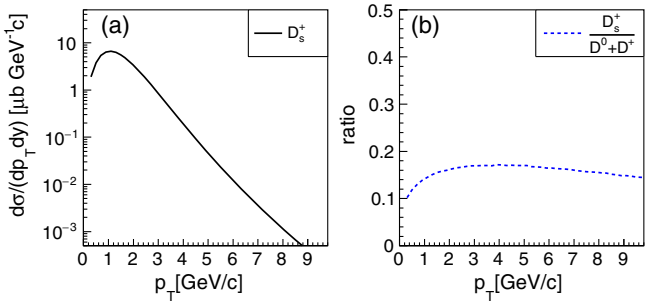

FIG. 5. Differential cross section of D_s^+ (a) and the spectrum ratio $D_s^+/(D^0 + D^+)$ (b) at midrapidity in pp collisions at $\sqrt{s} = 200$ GeV.

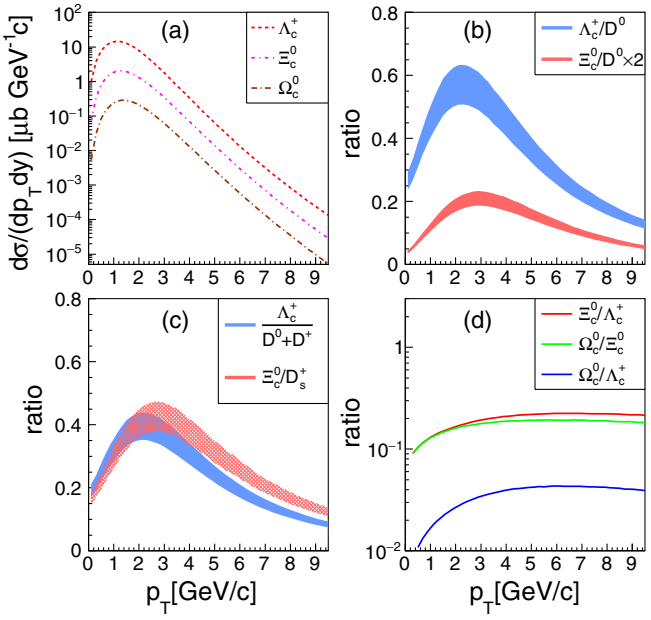

FIG. 6. Differential cross sections of Λ_c^+, Ξ_c^0, and Ω_c^0 (a) and several ratios among charmed hadrons (b–d) at midrapidity in pp collisions at $\sqrt{s} = 200$ GeV.

and the combination kinematics is slightly different for $c\bar{s}$ and $c\bar{u}$ pairs.

We further calculate the p_T spectra of single-charm baryons by the equal-velocity combination of a charm and two light-flavor quarks. In Fig. 6(a), we present the results for differential cross sections of Λ_c^+, Ξ_c^0, and Ω_c^0 at midrapidity as the model parameter $R_{B/M}^{(c)}$ is taken as 0.374 ± 0.042. In the quark combination mechanism, a charm can form a meson by picking up an antiquark or form a baryon by picking up two quarks. Since hadronization unitarity requires that a charm quark has to become a hadron at last, there exists competition between baryon formation and meson formation. In our model, such a nonperturbative competition dynamic is parametrized by $R_{B/M}^{(c)}$ and is tuned by experimental data. We fit the latest experimental data of Λ_c^+/D^0 at midrapidity in pp collisions at LHC energies [59,60] and obtain $R_{B/M}^{(c)} \approx 0.374 \pm 0.042$. Then, we use it to predict the production of single-charm baryons at midrapidity in pp collisions at $\sqrt{s} = 200$ GeV.

In Fig. 6(b), we present the spectrum ratios Λ_c^+/D^0 and Ξ_c^0/D^0 as a function of p_T. Two ratios increase at low p_T, saturate at $p_T \approx 2$–3 GeV/c, and decrease at larger p_T. We emphasize that this nonmonotonic p_T dependence is a typical signal of our model and is mainly caused by the kinematics of equal-velocity quark combination and the property of the p_T spectra of light-flavor quarks.

In Fig. 6(c), we present spectrum ratios $\Lambda_c^+/(D^0 + D^+)$ and Ξ_c^0/D_s^+ in order to better quantify the baryon-to-meson production competition for charm quark hadronization. Since $D^0 + D^+$ including strong and electromagnetic decays contains all $c\bar{u}$ and $c\bar{d}$ combination channels and Λ_c^+ contains all cuu, cud, and cdd combination channels, the yield ratio $\Lambda_c^+/(D^0 + D^+)$ directly relates to $R_{B/M}^{(c)}$ in the model

$$\frac{d\sigma_{\Lambda_c^+}/dy}{d\sigma_{D^0+D^+}/dy} = \frac{2}{2+\lambda_s} R_{B/M}^{(c)}. \tag{13}$$

The coefficient $2/(2+\lambda_s)$ is quite stable because, on the one hand, λ_s is usually small (e.g., $\lambda_s = 0.29$ obtained in the current study for minimum bias pp collisions at $\sqrt{s} = 200$ GeV), and on the other hand, the change of λ_s in different multiplicity classes in pp collisions is relatively small ($\Delta\lambda_s \lesssim 0.1$) according to our previous study of the multiplicity dependence of light-flavor hadrons [43] and experimental data for multiplicity dependence of the K/π ratio in pp collisions at $\sqrt{s} = 13$ TeV [61]. Therefore, the ratio $\Lambda_c^+/(D^0 + D^+)$ is a sensitive probe of the relative probability of cl_1l_2 combination against the $c\bar{l}$ combination (here, $l = u, d$) at charm quark hadronization. Similarly, $\Xi_c^0(cds)/D_s^+(c\bar{s})$ denotes the relative probability of the cds combination against the $c\bar{s}$ combination. Since the suppression influence of the strange quark is canceled in the ratio, we have $\Xi_c^0/D_s^+ = \Lambda_c^+/(D^0 + D^+)$ for yield ratios. In Fig. 6(c), we also see that the spectrum ratios $\Lambda_c^+/(D^0 + D^+)$ and Ξ_c^0/D_s^+ have the same magnitude. The small difference in p_T dependence between the two ratios is caused by the combination kinematics; i.e., momentum fractions x_u and x_s are different in combination with a charm quark.

In Fig. 6(d), we present ratios Ξ_c^0/Λ_c^+, Ω_c^0/Λ_c^+, and Ω_c^0/Ξ_c^0 as a function of p_T. In our model, they are related to the combination dynamics of an increasing number of strange quarks involving the combination process. Statistical combination symmetry is mainly used in the model and gives in yield ratios

$$\frac{d\sigma_{\Xi_c^0}/dy}{d\sigma_{\Lambda_c^+}/dy} = \frac{d\sigma_{\Omega_c^0}/dy}{d\sigma_{\Xi_c^0}/dy} = \frac{1}{2}\lambda_s, \tag{14}$$

$$\frac{d\sigma_{\Omega_c^0}/dy}{d\sigma_{\Lambda_c^+}/dy} = \frac{1}{4}\lambda_s^2 \tag{15}$$

where $\lambda_s = 0.29$ in pp collisions at $\sqrt{s} = 200$ GeV. We clearly see this flavor hierarchy property in spectrum ratios in Fig. 6(d). In addition, we see a p_T dependence for three ratios, which is because the difference between the p_T spectrum of up/down quarks and that of strange quarks at hadronization.

VI. SUMMARY AND DISCUSSION

In summary, we applied an equal-velocity quark combination model to understand the early RHIC data for p_T spectra of hadrons at midrapidity in pp collisions at $\sqrt{s} = 200$ GeV. We found explicit signals of a quark combination at hadronization. First, we observed a constituent quark number scaling property for the p_T spectra of Ω and ϕ and that of a proton and ρ. Second, based on the p_T spectrum of up/down quarks extracted from the proton data and that of strange quarks extracted from the ϕ data, we found that the data for the p_T spectra of Λ, Ξ^-, and K^{*0} are also well described. Third, based on the obtained spectrum of up/down quarks and a spectrum of charm quarks which is consistent with the theoretical calculations of the FONLL approach, we found that the experimental data for the differential cross section of D^{*+} are also well described.

Comparing these results in pp collisions at $\sqrt{s} = 200$ GeV with those in pp collisions at LHC energies in our previous works [42,43,45,46], we found a similarity in hadron production at hadronization at these two energy scales, which is exhibited as follows:

(1) Quark flavor correlation on p_T spectra of light-flavor hadrons at midrapidity in the low and intermediate p_T range.

Here, the low and intermediate p_T range denotes the range $p_T \lesssim 4$ GeV/c for mesons and $p_T \lesssim 6$ GeV/c for baryons. In our EVC mechanism, these hadrons are formed by soft (anti)quarks, i.e., $p_{T,q} \approx p_{T,h}/n_q \lesssim 2$ GeV/c ($n_q = 2$ for meson and $n_q = 3$ for baryon).

A typical signal of the correlation is the constituent quark number scaling property for experimental data of the p_T spectra of Ω and ϕ, which means that the formation of two hadrons shares the same strange quark source. In addition, as indicated by their p_T spectra at midrapidity, formation of K^*, Λ, and Ξ also shares the above strange quark source, and shares the same up/down quark source with that of protons.

(2) A connection between the p_T spectrum of D^* in the low and intermediate p_T range and soft light-flavor quarks that can form light-flavor hadrons.

Here, the low and intermediate p_T range for single-charm hadrons denotes the range $p_{T,h} \lesssim 8$ GeV/c. The light-favor (anti)quarks that take part in the formation of these single-charm hadrons have soft momentum $p_{T,q} \approx p_{T,c}/r_{cl} \lesssim 2$ GeV/c.

Our result for the p_T spectrum of D^{*+} indicates that the formation of D^{*+} shares the same down quark source with that of light-flavor hadrons. (In pp collisions at LHC energies, we found more such indications by other single-charm hadrons such as D^0, D_s^+, and Λ_c^+ [45,46]. We therefore predict the p_T spectra of these hadrons in pp collisions at $\sqrt{s} = 200$ GeV to further test this point by comparing with STAR experimental data in the future.) This similarity therefore indicates a universal scenario for production of hadrons in the low and intermediate p_T range in pp collisions at RHIC and LHC energies. At hadronization, we take constituent quarks and antiquarks as effective degrees of freedom for final parton system created in pp collisions. The equal-velocity combination is the main feature in hadronization processes of these constituent quarks and antiquarks. Equal-velocity combination of soft light-flavor (anti)quarks forms various light-flavor hadrons. Charm quarks are occasionally created, and some of them with relatively low momenta combine with the neighboring soft light-flavor (anti)quarks with the same velocity to form charm hadrons.

Moreover, we also have the similar finding in pPb and AA collisions in our recent works [41,44,62,63]. In particular, an equal-velocity combination mechanism is further tested by the elliptic flow of light-flavor hadrons in AA collisions at both RHIC and LHC energies [64]. Considering that the size of soft parton systems created in pp, pA, and AA collisions is quite different, it is natural to ask what underlying physics causes the same hadronization mechanism we found in these collisions. Does it relate to some essential feature of nonperturbative QCD and/or some particular structure of a final-state soft parton system? These questions deserve to be studied further in the future.

Finally, we suggest the systematic measurements in pp collisions at $\sqrt{s} = 200$ GeV in the future. These measurements should include ridge or long-range correlation, collectivity, multiplicity dependence of hadron production, and so on. By a systematic comparison with available LHC data, these measurements will greatly improve our understanding for the property of the small parton system created in pp collisions at different collision energies.

ACKNOWLEDGMENTS

We thank Z. B. Xu for helpful discussions. This work is supported in part by the Shandong Provincial Natural Science Foundation (Grants No. ZR2019YQ06 and No. ZR2019MA053), the National Natural Science Foundation of China under Grants No. 11975011 and No. 11805082, and the Higher Educational Youth Innovation Science and Technology Program of Shandong Province (Grant No. 2019KJJ010).

[1] B. Andersson, G. Gustafson, G. Ingelman, and T. Sjöstrand, Phys. Rep. **97**, 31 (1983).
[2] B. R. Webber, Nucl. Phys. **B238**, 492 (1984).
[3] J. D. Bjorken and G. R. Farrar, Phys. Rev. D **9**, 1449 (1974).
[4] K. P. Das and R. C. Hwa, Phys. Lett. **68B**, 459 (1977); **73B**, 504(E) (1978).
[5] K. Adcox *et al.* (PHENIX Collaboration), Phys. Rev. Lett. **88**, 242301 (2002).
[6] B. I. Abelev *et al.* (STAR Collaboration), Phys. Rev. Lett. **97**, 152301 (2006).
[7] J. Adams *et al.* (STAR and STAR RICH Collaborations), arXiv:nucl-ex/0601042.
[8] J. Adams *et al.* (STAR Collaboration), Phys. Rev. Lett. **92**, 052302 (2004).
[9] J. Adams *et al.* (STAR Collaboration), Phys. Rev. C **72**, 014904 (2005).
[10] A. Adare *et al.* (PHENIX Collaboration), Phys. Rev. Lett. **98**, 162301 (2007).
[11] V. Greco, C. M. Ko, and P. Lévai, Phys. Rev. Lett. **90**, 202302 (2003).
[12] R. J. Fries, B. Müller, C. Nonaka, and S. A. Bass, Phys. Rev. Lett. **90**, 202303 (2003).
[13] R. C. Hwa and C. B. Yang, Phys. Rev. C **67**, 034902 (2003).
[14] D. Molnar and S. A. Voloshin, Phys. Rev. Lett. **91**, 092301 (2003).
[15] L.-W. Chen and C. M. Ko, Phys. Rev. C **73**, 044903 (2006).
[16] C.-e. Shao, J. Song, F.-l. Shao, and Q.-b. Xie, Phys. Rev. C **80**, 014909 (2009).
[17] V. Khachatryan *et al.* (CMS Collaboration), J. High Energy Phys. 09 (2010) 091.
[18] S. Chatrchyan *et al.* (CMS Collaboration), Phys. Lett. B **718**, 795 (2013).
[19] V. Khachatryan *et al.* (CMS Collaboration), Phys. Rev. Lett. **115**, 012301 (2015).
[20] V. Khachatryan *et al.* (CMS Collaboration), Phys. Lett. B **765**, 193 (2017).
[21] J. Adam *et al.* (ALICE Collaboration), Nat. Phys. **13**, 535 (2017).
[22] B. B. Abelev *et al.* (ALICE Collaboration), Phys. Lett. B **728**, 25 (2014).
[23] J. Adam *et al.* (ALICE Collaboration), Phys. Lett. B **760**, 720 (2016).
[24] J. Adam *et al.* (ALICE Collaboration), Phys. Lett. B **758**, 389 (2016).
[25] S. K. Prasad, V. Roy, S. Chattopadhyay, and A. K. Chaudhuri, Phys. Rev. C **82**, 024909 (2010).
[26] F.-M. Liu and K. Werner, Phys. Rev. Lett. **106**, 242301 (2011).
[27] A. Bzdak, B. Schenke, P. Tribedy, and R. Venugopalan, Phys. Rev. C **87**, 064906 (2013).
[28] P. Bozek and W. Broniowski, Phys. Rev. C **88**, 014903 (2013).
[29] E. Avsar, C. Flensburg, Y. Hatta, J.-Y. Ollitrault, and T. Ueda, Phys. Lett. B **702**, 394 (2011).
[30] W. Zhao, Y. Zhou, H. Xu, W. Deng, and H. Song, Phys. Lett. B **780**, 495 (2018).
[31] T. Sjöstrand, Adv. Ser. Dir. High Energy Phys. **29**, 191 (2018).
[32] A. Ortiz Velasquez, P. Christiansen, E. Cuautle Flores, I. Maldonado Cervantes, and G. Paić, Phys. Rev. Lett. **111**, 042001 (2013).
[33] C. Bierlich, G. Gustafson, L. Lönnblad, and A. Tarasov, J. High Energy Phys. 03 (2015) 148.
[34] C. Bierlich and J. R. Christiansen, Phys. Rev. D **92**, 094010 (2015).
[35] I. Bautista, A. F. Téllez, and P. Ghosh, Phys. Rev. D **92**, 071504 (2015).
[36] J. R. Christiansen and P. Z. Skands, J. High Energy Phys. 08 (2015) 003.
[37] N. Fischer and T. Sjöstrand, J. High Energy Phys. 01 (2017) 140.
[38] S. Gieseke, P. Kirchgaeßer, and S. Plätzer, Eur. Phys. J. C **78**, 99 (2018).
[39] A. Andronic, P. Braun-Munzinger, M. K. Köhler, A. Mazeliauskas, K. Redlich, J. Stachel, and V. Vislavicius, J. High Energy Phys. 07 (2021) 035.
[40] F.-l. Shao, G.-j. Wang, R.-q. Wang, H.-h. Li, and J. Song, Phys. Rev. C **95**, 064911 (2017).
[41] J. Song, X.-r. Gou, F.-l. Shao, and Z.-T. Liang, Phys. Lett. B **774**, 516 (2017).
[42] X.-r. Gou, F.-l. Shao, R.-q. Wang, H.-h. Li, and J. Song, Phys. Rev. D **96**, 094010 (2017).
[43] J.-w. Zhang, H.-h. Li, F.-l. Shao, and J. Song, Chin. Phys. C **44**, 014101 (2020).
[44] H.-H. Li, F.-L. Shao, J. Song, and R.-Q. Wang, Phys. Rev. C **97**, 064915 (2018).
[45] J. Song, H.-h. Li, and F.-l. Shao, Eur. Phys. J. C **78**, 344 (2018).
[46] H.-h. Li, F.-l. Shao, and J. Song, Chin. Phys. C **45**, 113105 (2021).
[47] J. Adams *et al.* (STAR Collaboration), Phys. Lett. B **612**, 181 (2005).
[48] J. Adams *et al.* (STAR Collaboration), Phys. Rev. Lett. **92**, 092301 (2004).
[49] J. Adams *et al.* (STAR Collaboration), Phys. Rev. C **71**, 064902 (2005).
[50] B. I. Abelev *et al.* (STAR Collaboration), Phys. Rev. C **75**, 064901 (2007).
[51] J. Adams *et al.* (STAR Collaboration), Phys. Lett. B **637**, 161 (2006).
[52] L. Adamczyk *et al.* (STAR Collaboration), Phys. Rev. D **86**, 072013 (2012).
[53] H. Qiu (STAR Collaboration), Nucl. Part. Phys. Proc. **276–278**, 213 (2016).
[54] M. Cacciari, M. Greco, and P. Nason, J. High Energy Phys. 05 (1998) 007.
[55] M. Cacciari, S. Frixione, and P. Nason, J. High Energy Phys. 03 (2001) 006.
[56] R. Aaij *et al.* (LHCb Collaboration), J. High Energy Phys. 03 (2016) 159; 09 (2016) 013(E); 05 (2017) 074(E).
[57] S. Acharya *et al.* (ALICE Collaboration), Eur. Phys. J. C **77**, 550 (2017).
[58] S. Acharya *et al.* (ALICE Collaboration), Eur. Phys. J. C **79**, 388 (2019).

[59] S. Acharya *et al.* (ALICE Collaboration), Phys. Rev. C **104**, 054905 (2021).
[60] S. Acharya *et al.* (ALICE Collaboration), Phys. Rev. Lett. **128**, 012001 (2022).
[61] S. Acharya *et al.* (ALICE Collaboration), Eur. Phys. J. C **80**, 693 (2020).
[62] J. Song, X.-F. Wang, H.-H. Li, R.-Q. Wang, and F.-L. Shao, Phys. Rev. C **103**, 034907 (2021).
[63] R.-Q. Wang, J. Song, F.-L. Shao, and Z.-T. Liang, Phys. Rev. C **101**, 054903 (2020).
[64] J. Song, H.-h. Li, and F.-l. Shao, Eur. Phys. J. C **81**, 1 (2021).